1995

Three-dimensional instabilities of film flows

Jun Liu

J. B. Schnieder

Jerry P. Gollub
Haverford College

Threedimensional instabilities of film flows

Jun Liu, J. B. Schneider, and J. P. Gollub

Citation: Phys. Fluids **7**, 55 (1995); doi: 10.1063/1.868782
View online: http://dx.doi.org/10.1063/1.868782
View Table of Contents: http://pof.aip.org/resource/1/PHFLE6/v7/i1
Published by the American Institute of Physics.

Three-dimensional instabilities of film flows

Jun Liu, J. B. Schneider, and J. P. Gollub
Department of Physics, Haverford College, Haverford, Pennsylvania 19041 and Department of Physics, University of Pennsylvania, Philadelphia, Pennsylvania 19104

(Received 6 June 1994; accepted 20 September 1994)

Two-dimensional (2-D) interfacial waves on flowing films are unstable with respect to both two- and three-dimensional instabilities. In this paper, several distinct three-dimensional instabilities that occur in different regions of the parameter space defined by the Reynolds number R and the frequency f of forced two-dimensional waves are discussed in detail. (a) *A synchronous 3-D instability*, in which spanwise deformations of adjacent wave fronts have the same transverse phase, appears over a wide range of frequency. These transverse modulations occur mainly along the troughs of the primary waves and eventually develop into sharp and nearly isolated depressions. The instability involves many higher harmonics of the fundamental 2-D waves. (b) A *3-D surbharmonic instability* occurs for frequencies close to the neutral curve $f_c(R)$. In this case, the transverse modulations are out of phase for successive wave fronts, and herringbone patterns result. It is shown that this weakly nonlinear instability is due to the resonant excitation of a triad of waves consisting of the fundamental two-dimensional wave and two oblique waves. The evolution of wavy films after the onset of either of these 3-D instabilities is complex. However, sufficiently far downstream, large-amplitude solitary waves absorb the smaller waves and become dominant. © *1995 American Institute of Physics.*

I. INTRODUCTION

Thin liquid films flowing down an incline provide a useful opportunity to study the development of spatial complexity through successive bifurcations.[1–3] Flowing films are unstable to sufficiently long-wavelength perturbations when the Reynolds number exceeds a critical value. The resulting interfacial waves show a wide variety of nonlinear wave phenomena. Well-developed wavy films are three dimensional,[1,4–6] though the initial waves are two dimensional near their onset (i.e., invariant in the spanwise direction). The transition to three-dimensionality has not been documented experimentally in the literature.

The evolution from two- to three-dimensional film flows is analogous to the transitional phenomena that are well known in various shear flows.[7–11] The investigation of these processes in the context of film flows may shed some light on shear flow instabilities in general, since the instability mechanisms may be related.

In this paper, we report an experimental investigation of three-dimensional (3-D) secondary instabilities of flowing films, as part of an effort to understand their transition to complex disordered patterns. (Some preliminary results were published previously in Ref. 12.) In the next section, we review previous work on the secondary instability of film flows, and discuss the relevant literature on 3-D instabilities of boundary layers. Our experimental setup and measurement methods are briefly described in Sec. III. In Sec. IV, the experimental results are presented. We give a general picture of 3-D instabilities by reporting a stability diagram in the parameter space defined by Reynolds number and the frequency of the initial two-dimensional (2-D) waves. Several distinct transverse instabilities are found to deform the traveling waves: a synchronous mode (in which the deformations of adjacent wave fronts are in phase) and a subharmonic mode (in which the modulations of adjacent wave fronts are out of phase). A detailed study of these instabilities is then presented, along with a qualitative treatment of the further evolution toward an asymptotic "turbulent" regime.

II. BACKGROUND

A. Secondary instability of film flows

The important parameters of film flows are (a) the Reynolds number $R=h_0u_0/\nu$, based on the unperturbed film thickness h_0, the fluid velocity u_0 at the surface, and the kinematic viscosity ν; and (b) the Weber number $W=\gamma/(\rho h_0^2 g \sin\beta)$, where γ is the surface tension, ρ is the density of the fluid, g is the gravitational acceleration, and β is the inclination angle that the film plane makes with the horizontal. The surface velocity of a flat film is $u_0=gh_0^2 \sin\beta/(2\nu)$. The critical Reynolds number for the primary instability is given[13,14] by $R_c=\frac{5}{4}\cot\beta$. The primary instability is convective (in the sense that disturbances grow only in some moving frames of Ref. 15), and the resulting waves are sensitive to noise near the source.[16,17]

Because 2-D disturbances grow more rapidly than 3-D ones,[18–20] two-dimensional waves with straight wave fronts are selectively amplified by the primary instability. The nonlinear evolution of periodic 2-D waves depends strongly on the frequency f, as determined by small perturbations near the inlet. Isolated *solitary waves* appear at low frequencies, while saturated finite-amplitude waves occur at high frequencies.[6,16,21] (These solitary waves should not be confused with *solitons*, because the former are interacting and dissipative.) Sufficiently far downstream, complex disordered patterns develop, and the waves eventually become statistically independent of perturbations near the source. The transition process involves various two- and three-dimensional secondary instabilities.

For relatively high viscosity and low R, transverse

modulations are usually suppressed, and periodic 2-D waves are unstable primarily *to streamwise* perturbations. We showed in Ref. 22 that the 2-D secondary instability is also convective. Both subharmonic and sideband 2-D instabilities were found, but in different ranges of frequency. The 2-D sideband instability predominates for waves close to the cutoff (neutral) frequency $f_c(R)$, while the 2-D subharmonic instability appears at lower frequencies. Recent theoretical treatments[23,24] agree qualitatively with our observations.

At lower viscosities and higher R, the wave fronts are subject to 3-D transverse instabilities.[5] Synchronous modulations and herringbone patterns were observed qualitatively in our preliminary experiments.[12] For the synchronous 3-D instability, the periodicity in the streamwise direction is the same as that of the fundamental waves. However, the herringbone pattern doubles the period of 2-D waves, and the phase of the transverse modulation differs by π for successive wave fronts. The regions in parameter space where these instabilities occur were not explored in the earlier work, and the mechanisms responsible for the instabilities were unknown.

The 3-D secondary instabilities have been studied theoretically and numerically by several groups. Krishna and Lin[20] first examined the stability of monochromatic waves near $f_c(R)$ with respect to 3-D sideband perturbations by using a long wave evolution equation. They found that these monochromatic waves are stable if the perturbation wave vector is sufficiently close to the fundamental. Cheng and Chang[25] later showed that relatively long waves may be unstable to a transverse sideband instability. Using Floquet analyses, Joo and Davis[17] and Trifonov[26] studied the synchronous and subharmonic 3-D instabilities numerically. Joo and Davis found that supercritically saturated waves near $f_c(R)$ are subject to a synchronous instability, with sufficiently long spanwise wavelengths. At least for vertical films, this instability does not require a threshold amplitude of 2-D waves. Trifonov's calculations illustrated that the 3-D subharmonic instability leads to a checkerboard pattern of wave maxima. He also predicted some qualitative differences in the breakdown patterns between solitary waves driven at low frequency on the one hand, and waves close to the neutral curve on the other.

Chang *et al.*[23] recently showed that nearly sinusoidal waves are unstable to a 3-D subharmonic instability in the presence of significant transverse noise. The instability results from the resonant excitation of a triad of waves consisting of the fundamental 2-D wave and two oblique waves. The streamwise component of the wave number of the oblique waves is the subharmonic of the fundamental. This three-wave interaction is predicted to produce a herringbone pattern, as observed in our preliminary report.[12] We test this idea in the present work.

B. Three-dimensional instability of boundary layers

Three-dimensional instabilities have been intensively studied in boundary layers[9–11] and other shear layers.[7,8] There is much evidence that similar physical mechanisms can operate in various shear flows, so it is helpful to look briefly at the 3-D instabilities of boundary layers before presenting the results on film flows. However, we do not mean to imply that the instability modes (and mechanisms) of film flows[27,28] are the same as those of shear layers.

For Tollmien–Schlichting (TS) waves in boundary layers, two types of 3-D transitions have been found: the "K-type" transition,[29] in which the amplitude of velocity fluctuations is synchronously modulated in the spanwise direction; and 3-D subharmonic resonance.[11,30] The K-type transition appears whenever the TS wave amplitude exceeds a threshold, and is characterized by the appearance of *aligned* Λ-shaped vortices.[10] The 3-D subharmonic instability, on the other hand, can occur at smaller amplitude, and is characterized by *staggered* Λ-shaped vortices.

Several theoretical approaches were developed in the study of 3-D instabilities, including the weakly nonlinear method and Floquet analysis. Both involve *resonances*, but with different physical interpretations.[31] The weakly nonlinear theory of the 3-D instability begins with a resonant triad model,[32,33] in which a primary 2-D wave $(\mathbf{k},f)$ interacts strongly with a pair of oblique waves $(\mathbf{k}_1,f_1)$ and $(\mathbf{k}_2,f_2)$ when they satisfy the conditions of phase synchronism: $\mathbf{k}=\mathbf{k}_1+\mathbf{k}_2$, and $f=f_1+f_2$, where $\mathbf{k}$ is the wave vector. The three-wave interaction corresponds to the lowest-order nonlinear (quadratic) term in the amplitude equations. It has been shown that the weakly nonlinear theory agrees quantitatively with the experimental observations of 3-D subharmonic excitation of TS waves.[11,34] However, this theory cannot explain the K-type transition.

Another approach is to analyze the linear stability of a spatially periodic 2-D flow with respect to ambient 3-D disturbances by using the Floquet theorem.[10,31] A detailed summary of this method can be found in Herbert's review.[10] The Floquet analysis provides a useful portrait of the 3-D secondary instability. Its predictions also show quantitative agreement with experiments on the 3-D subharmonic transition in boundary layers.[10,11]

The nature of the K-type transition turns out to be much more complicated than the 3-D subharmonic transition because of its strong nonlinearity. (We find a similar dichotomy for the two instabilities discussed in this paper.) Kachanov[11,35] recently proposed that the K-type transition is due to a cascade of wave resonances in which a large number of higher harmonics are involved.

III. EXPERIMENTAL METHODS

Our flow and measurement systems are briefly described here; a detailed description can be found in our previous papers.[16,21] The film plane is 200 cm long by 50 cm transverse to the flow; the inclination angle β may be varied continuously over the range 0°–35°. The entrance flow rate can be perturbed at frequency f by applying small pressure variations to the entrance manifold. Both pure water (ν=1.0 cS) and several aqueous solution of glycerin (ν=2–3 cS) are used in the experiment. The results presented in this paper are based primarily on a solution with 31% glycerin by weight. Its density, kinematic viscosity, and surface tension are measured to be ρ=1.07 g/cm^3, ν=2.3 cS and γ=67 dyn/cm, respectively, at 22 °C. The working temperature varies by less than 0.4 °C in a few hours. We check the surface

tension and viscosity regularly, and have confirmed that glycerin solutions are less affected by adsorbed surfactants than is pure water.[6]

A fluorescence imaging method[16] is used to measure the relative film thickness $h(x,y,t)/h_0$ in real time with measurement precision of about 1%, which corresponds to 10 μm for 1 mm thick film, where x, y are the streamwise and spanwise coordinates. (We define $x=0$ at the inlet.) To perform this measurement, we dope the fluid with a small concentration (100–200 ppm) of dye that fluoresces under ultraviolet light, and digitize the resulting images taken by a shuttered high-resolution CCD camera. The fluorescence intensity is proportional to the thickness for films in the relevant range of thickness.[21] For periodic waves, phase-sensitive averaging is used to improve the measurement sensitivity to 3–4 μm.[16] We can acquire imaging data at 30 Hz or localized data at 60 Hz using the interlaced camera and an imaging board with dual-port memory.

We also measure the local wave slope $s(x_o,t)$ by laser beam deflection.[16] The fractional sensitivity of this method is about 5×10^{-5}, which corresponds typically to wave amplitudes of about 0.5 μm.

When studying the onset of 3-D instabilities, we need to determine the slow spatial variation of wave structures. Therefore, we use small inclination angles ($\beta=2.5°-7°$) and moderate Reynolds numbers ($R<100$) in this experiment.

Primary 2-D waves amplified from ambient noise are not very regular. To discover the individual mechanisms leading to three-dimensionality, we study the instability of *periodic* 2-D waves, which are introduced by perturbing the entrance flow rate with sinusoidal pressure vibrations. For a fixed inclination angle (β) and a particular fluid, the independent experimental parameters are R and the primary wave frequency f. (The Weber number W depends on the fluid properties and on R, so it is not independent.) The sources of irregularity that are amplified by the 3-D instabilities include both ambient noise and slight imperfections of the entrance manifold.

IV. RESULTS

Finite-amplitude 2-D waves are generally unstable to 3-D secondary instabilities. In this section, we first describe the 3-D instabilities observed in our experiments qualitatively, and report a stability phase diagram measured in R vs f space. Detailed studies of each of these 3-D instabilities are then presented. Finally, we describe qualitatively the further evolution of wavy films after the onset of three-dimensional instabilities.

A. Three-dimensional secondary instabilities—Qualitative summary

Patterns arising from two distinct 3-D instabilities have been identified in our experiments: synchronous transverse modulations and herringbone patterns. For the synchronous 3-D pattern, the periodicity in the streamwise direction is the same as that of the primary 2-D waves. The herringbone pattern, on the other hand, doubles the period of 2-D waves, and the phase of the transverse modulations differs by π for adjacent wave fronts. The 3-D instability mechanism depends strongly on the structure of the finite-amplitude 2-D waves, and therefore on f and R.

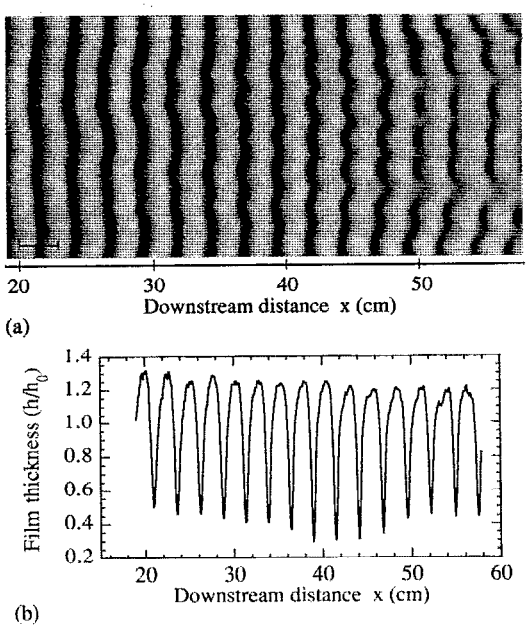

FIG. 1. Synchronous 3-D instability of 2-D periodic waves. (a) A snapshot taken at $\beta=6.4°$, $R=72$, and $f=10.0$ Hz. The bar corresponds to 3 cm. (b) The wave profile read from the centerline of (a). The film thickness is normalized by the average thickness h_0 of the unforced film. The 2-D waves are far from sinusoidal.

A typical example of the synchronous instability is shown in Fig. 1(a), a snapshot taken at $\beta=6.4°$, $R=72$, and $f=10$ Hz by the fluorescence imaging method. The gray scale of the image is proportional to the film thickness, i.e., the thick region is bright and the thin region is dark. Figure 1(b) shows the wave profile along the centerline of Fig. 1(a). When a 2-D wave becomes large, transverse modulations appear and grow downstream. At $x\approx40$ cm, nearly periodic spanwise modulations are visible. The modulations take place mainly along the troughs (or valleys) of the 2-D waves. The spanwise wavelength is comparable to the streamwise wavelength. As the waves travel farther downstream ($x>50$ cm), the 2-D wave fronts begin to break, and each valley develops into a row of nearly isolated depressions. Subsequently, the flow becomes disordered.

The primary 2-D waves shown in Fig. 1 are *single peaked* (one peak per period), and have quite flat maxima and steep dips [Fig. 1(b)]. However, *solitary waves*[6,16,21] occur at very low f (Fig. 2). A solitary wave is composed of a large maximum preceded by several subsidiary maxima. Solitary waves are also unstable to transverse modulations [Fig. 2(a)]. The spanwise wavelength (~3 cm) shown in Fig. 2 is significantly smaller than the spacing of the solitary waves (~21 cm). The transverse modulations saturate and do not result in disconnected wave fronts. The curvature of the 2-D wave fronts is due to boundary effects.[16] It does not affect the above transverse instability, since the spanwise wavelength is much smaller than the width of film plane. Farther downstream, the modulations sometimes become

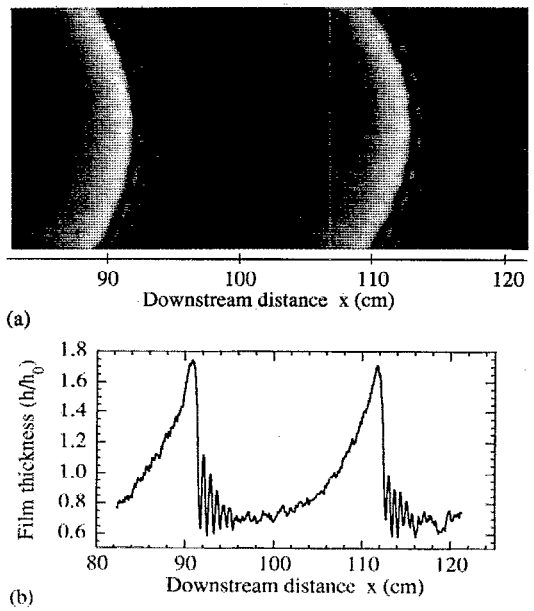

FIG. 2. Spanwise modulations of solitary waves. (a) A snapshot taken at $\beta=4.0°$, $R=73$, and $f=1.4$ Hz. Transverse modulations distort the steep fronts of solitary waves and the subsidiary wave fronts. (b) The wave profile read from the centerline of (a). The wavelength of the solitary waves is about 21 cm.

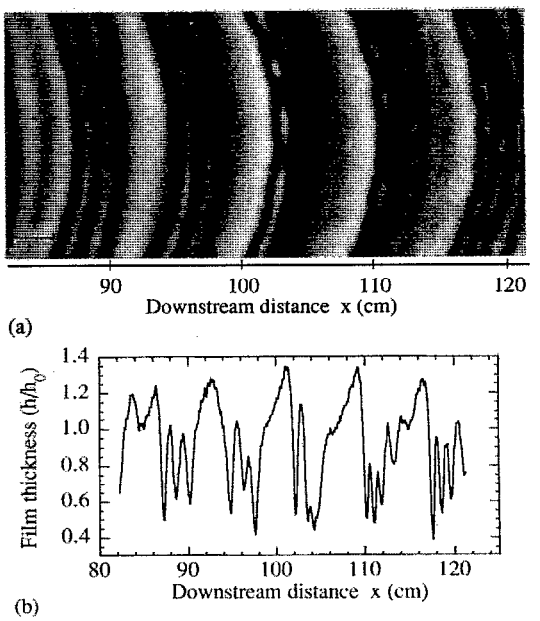

FIG. 3. Transverse instability of multipeaked waves at an intermediate frequency. (a) A snapshot taken at $\beta=4.0°$, $R=62$, and $f=3.0$ Hz. The spanwise modulations and the interactions between the primary and subsidiary wave fronts occur in the same region. (b) The wave profile read from the centerline of (a).

weaker. Because of the finite length of the film plane, we cannot systematically study the ultimate stability of solitary waves.

When f is increased to a value between those of Figs. 1 and 2, the primary wave fronts are closer together, and separate solitary waves cannot be formed (Fig. 3). This leads to a strong interaction between primary and subsidiary wave fronts.[21] As shown in Fig. 3, the transverse instability of multipeaked waves often occurs simultaneously, so that the overall structure is fairly complex. Traveling downstream, the wavering 2-D wave fronts become unstable to a mixture of streamwise perturbations and spanwise phase modulations.

The instabilities documented in Figs. 1–3 are all classified as examples of the *synchronous* 3-D instability because they do not alter the period (or wave number) of the basic 2-D waves until a later stage. The power spectra (not shown) of the local film thickness $h(x_0,y_0,t)$ primarily reveal the fundamental frequency and its higher harmonics.

A quite different 3-D instability can appear when f is larger and close to $f_c(R)$; an example is shown in Fig. 4. In this case, initial periodic 2-D waves are nearly sinusoidal [Fig. 4(b)]. The transverse phase of the modulations differs by π for successive wave fronts, and the streamwise period is doubled [Fig. 4(a)]. This generates a *herringbone* (or checkerboard) *pattern* that is similar to the staggered A-shaped vortices in shear layers. The herringbone patterns usually appear in patches and their location fluctuates in time.

The herringbone patterns are caused by a 3-D subharmonic instability. To verify this, we measured the power spectra of the local film thickness simultaneously at several positions along the centerline by using the fluorescence imaging method. Figure 5 gives the results for Fig. 4. At $x=76$ cm, the waves are two dimensional; the spectra show primarily the fundamental frequency and its harmonics [Fig. 5(a)]. At $x=105$ cm, herringbone patterns have developed; a

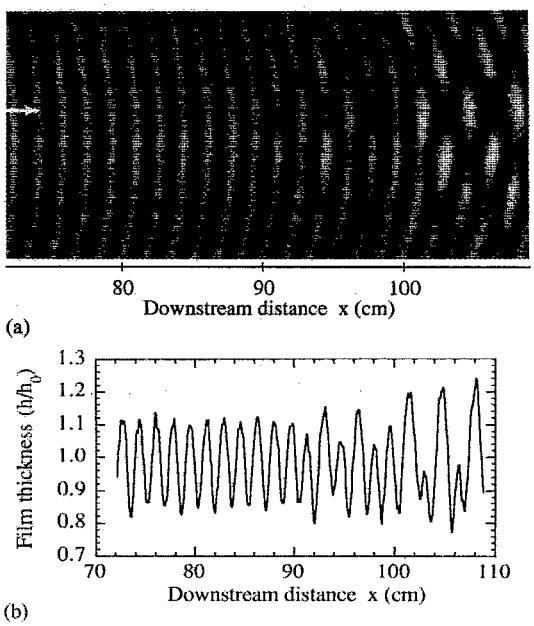

FIG. 4. Herringbone patterns due to the 3-D subharmonic instability. (a) A snapshot taken at $\beta=4.0°$, $R=50.5$, and $f=14.0$ Hz. (b) The wave profile read from the line indicated by the white arrow in (a). This line goes through a row of maxima.

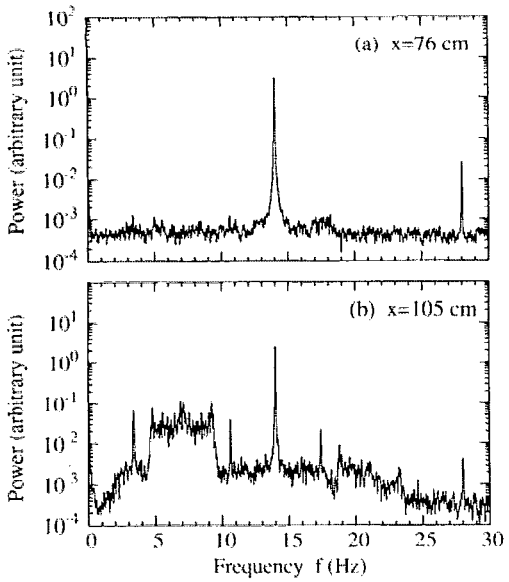

FIG. 5. Power spectra of local film thickness measured at two positions on the centerline of Fig. 4. (a) $x=76$ cm, where the transverse modulations are very small; (b) $x=105$ cm, where the herringbone pattern is well developed. The broad subharmonic resonance is evident.

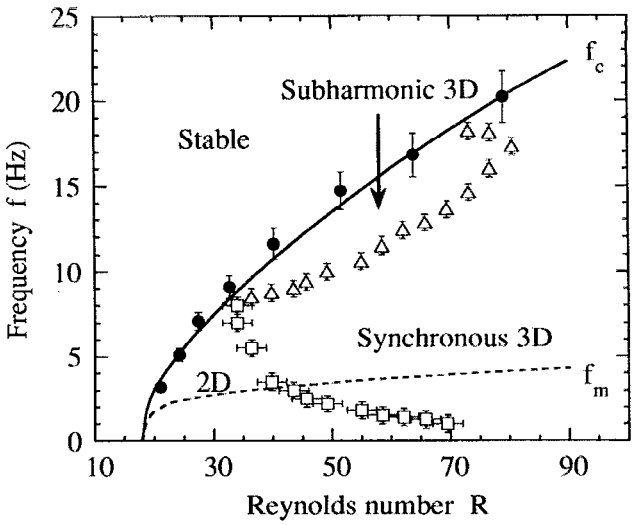

FIG. 6. Three-dimensional secondary instability phase diagram for $\beta=4.0°$, $\rho=1.07$ g/cm^3, $\nu=2.3$ cS, and $\gamma=67$ dyn/cm. The solid and dashed lines $f_c(R)$ and $f_m(R)$ are the neutral stability curve and the most amplified frequency for primary 2-D waves. The solid circles are the measurements of $f_c(R)$. The open squares give the measurements of $f_3(R)$ [or $R_3(f)$], below which no 3-D instability can be observed on our 2 m long plane. In the region enclosed by open triangles and $f_c(R)$, herringbone patterns can be observed. The synchronous 3-D instability is seen over a large range of frequency.

broadband at low frequency appears around the subharmonic [Fig. 5(b)]. Two extra peaks at 3.4 and 10.6 Hz of nearly equal strength also appear in the spectra. [These two peaks and the fine structure of the broadband in Fig. 5(b) are probably due to fluctuating disturbances of very small amplitude near the inlet. The structures are not exactly the same from run to run.]

Herringbone patterns are sensitive to initial conditions. This observation suggests that the 3-D subharmonic instability is convective. If strong transverse modulations somehow occur, well-defined herringbone patterns cannot be seen; they sometimes mix with other 3-D structures, or are significantly twisted, or just do not appear. However, this type of instability can be enhanced by applying controlled perturbations, as we discuss in Sec. IV C.

We have tried to explore all possible 3-D secondary instabilities in the parameter space defined by R and f. Although the different instabilities sometimes occur in combination, we have clearly identified two basic scenarios leading to three-dimensionality: the synchronous and subharmonic instabilities. The results are summarized in the 3-D instability phase diagram presented in Fig. 6. The solid and dashed lines $f_c(R)$ and $f_m(R)$ are, respectively, the neutral stability curve and the most amplified frequency predicted for primary 2-D waves by the linear stability theory. The solid circles are the measurements of $f_c(R)$. The curve $f_m(R)$ has also been confirmed experimentally.[21,36]

There seems to exist a "critical" frequency $f_3(R)$ [or equivalently, a critical Reynolds number $R_3(f)$] for the onset of 3-D instabilities. If $f<f_3(R)$ [or $R<R_3(f)$], 3-D instabilities are not observed on our *finite* film plane. This threshold has been determined by observation and is shown in Fig. 6 by open squares. We do not know whether such a stability boundary exists in a rigorous sense; it may be dependent on

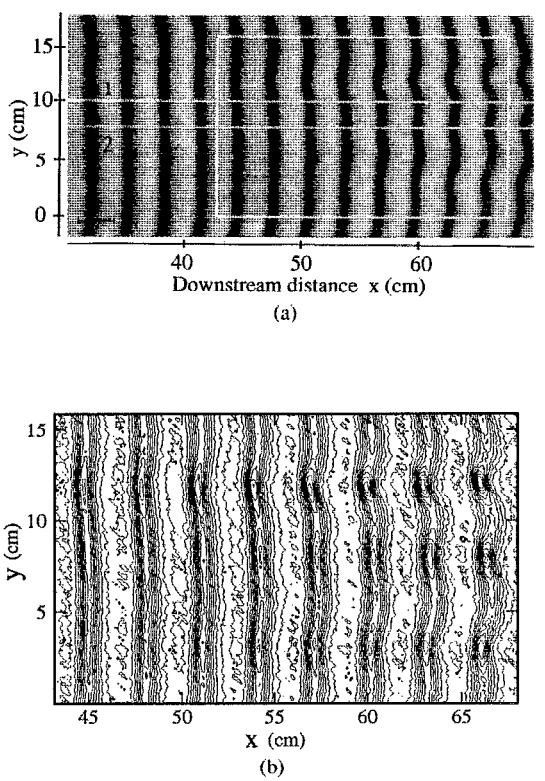

FIG. 7. Evolution of synchronous transverse modulations: (a) A snapshot taken at $\beta=4.0°$, $R=64$, and $f=7.0$ Hz. (Here $y=0$ is defined as the bottom line of the box.) (b) The isothickness contours show the film structure inside the box in (a). The thickness interval ($\Delta h/h_0$) between two neighboring contours is approximately 0.06. Lines 1 and 2 in (a) are marked for use in Fig. 8. Line 1 is the centerline *between* two trains of depressions. Line 2 goes through a train of depressions.

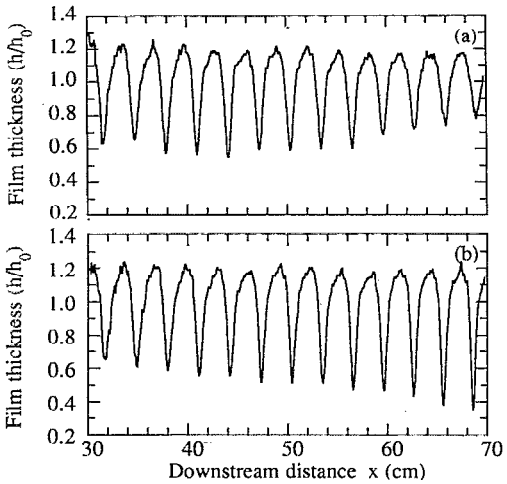

FIG. 8. Wave profiles read from (a) line 1 and (b) line 2 in Fig. 7. Note the quite different variation of the minima with downstream distance in the two cases.

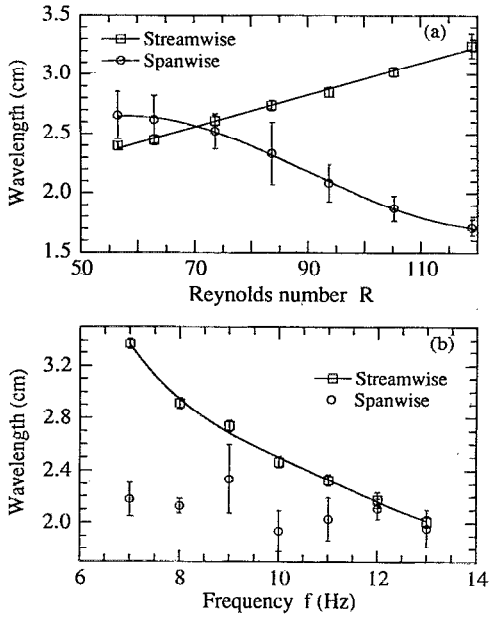

FIG. 10. Variation of streamwise and spanwise wavelengths (a) as a function of R for a fixed primary wave frequency $f=9$ Hz, and (b) as a function of f for a fixed $R=84$. The solid lines are guides to the eye ($\beta=6.4°$).

system size. However, $f_3(R)$ is useful in order to illustrate the relative importance of 3-D instabilities in different parameter regions. Only two-dimensional secondary instabilities[22] are detected for $f<f_3(R)$. Our experiments also suggest that $f_3(R)$ increases with viscosity, and decreases with inclination angle.

B. Synchronous three-dimensional instability

1. Observations

In this section, we focus on the synchronous instability shown in Fig. 1, where we can clearly separate the 3-D instability from other interactions. Our goal is to understand the important features of this instability and to determine appropriate ways to characterize it.

The synchronous 3-D instability develops spatially. In contrast to the 2-D secondary instabilities,[22] the inception of synchronous transverse modulations does not fluctuate in space and time if the primary waves are forced periodically. The local film thickness $h(x_0,y_0,t)$ remains periodic in time with the frequency of the fundamental waves until rather late in the development of the spanwise modulations. This observation suggests that the modulations originate from time-independent geometrical irregularities in the entrance manifold. (To demonstrate that the synchronous 3-D instability is convective, we would need to generate pulse-like transverse modulations. This turned out to be quite difficult.)

We now consider the example shown in Fig. 7(a). At $x\approx30$ cm, the waves are two dimensional. As they travel downstream, spanwise modulations grow gradually. The evolution of transverse modulations is illustrated more clearly in Fig. 7(b), which shows isothickness contours of the film inside the box given in (a). This instability significantly modulates the thickness along the deep troughs of initially 2-D waves. The resulting depressions travel slightly slower and distort the 2-D wave fronts. However, the flat peaks are hardly modulated transversely.

In Fig. 8, we plot two wave profiles $h(x,y_0)$ for the lines

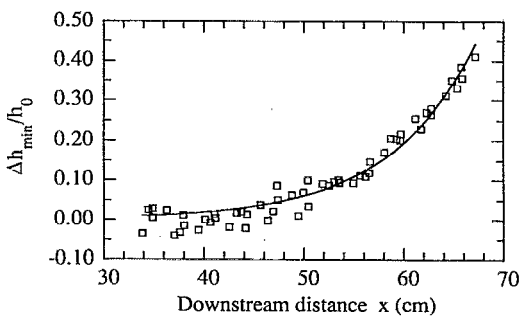

FIG. 9. Measurements of the trough transverse modulation amplitude $\Delta h_{\min}$ (see the text) between lines 1 and 2 in Fig. 7. The data are taken from many snapshots and normalized by h_0. The solid curve is an exponential fit.

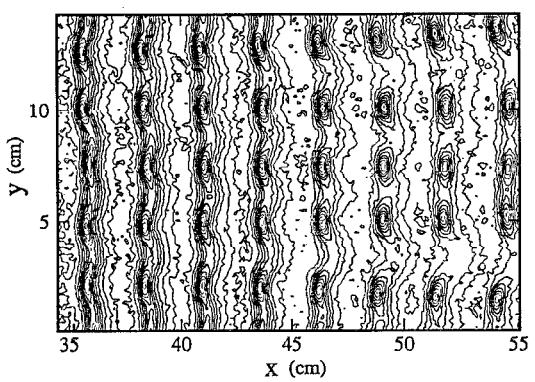

FIG. 11. Evolution of isolated depressions from the synchronous 3-D instability, as shown by isothickness contours. The thickness interval ($\Delta h/h_0$) between two neighboring contours is approximately 0.08 ($\beta=6.4°$, $R=72$, and $f=10.0$ Hz).

marked in Fig. 7(a). Line 1 [Fig. 8(a)] follows the centerline between two trains of depressions, while line 2 [Fig. 8(b)] goes directly through a train of depressions. As the waves move downstream, the troughs become shallower along line 1 and deeper along line 2. The intersections between line 1 and the troughs become *saddle points*, which are local minima in the streamwise direction but local maxima in the spanwise direction. The peak height decreases by a very small amount along both sampled lines, since the modulations extract energy from the waves. We can use the thickness difference between a depression and a neighboring saddle point of the same trough to characterize the spanwise modulation. This difference is called the *trough transverse modulation amplitude* and denoted as $\Delta h_{\min}$.

The measurements of $\Delta h_{\min}(x)$ between lines 1 and 2 in Fig. 7(a) are presented in Fig. 9. We fitted the data to an exponentially growing function (solid curve), and found a satisfactory fit: the spatial growth rate δ_i of $\Delta h_{\min}$ is $\delta_i \approx 0.11$ cm^{-1}. However, this growth rate must be interpreted cautiously, since it is not associated with a spanwise Fourier mode; the distortion is not sinusoidal. We measured the growth rate δ_i of transverse modulations as a function of f under the same experimental conditions as in Fig. 7, and found it varies by less than $\pm 5\%$ over the range 6–13 Hz. Similarly, we measured the transverse modulation amplitude along the wave maxima, and found it to be essentially zero. *This means that the transverse modulations are essentially confined to the trough (shallow) regions of the waves.*

Spontaneous transverse modulations often appear nearly periodic (Figs. 1 and 7). The spanwise wavelength is comparable to the streamwise wavelength of the fundamental waves. To understand the spanwise wavelength selection, we measured both the streamwise and spanwise wavelengths as functions of f and R. For fixed f, the streamwise wavelength (λ_x) increases with R, while the spanwise wavelength (λ_y) decreases [Fig. 10(a)]. Surprisingly, the spanwise wavelength does *not* seem to change with frequency for fixed R [Fig. 10(b)].[37]

The development of the synchronous instability does not lead to any quasistationary states. When the transverse modulations are well developed, the depressions stop deepening, while the saddle points keep rising. This process produces sharp and nearly isolated depressions that can persist for quite a long distance. We illustrate the process by plotting isothickness contours in Fig. 11. *Eventually, the troughs begin to separate into isolated depressions.*

Summary: The synchronous transverse modulations occur mainly along the troughs of the primary 2-D waves, and eventually develop into sharp and nearly isolated depressions. The spanwise wavelength is much longer than the film thickness and is comparable to the streamwise wavelength for moderate R.

2. Theoretical description of the synchronous instability

What are the mechanisms responsible for the synchronous instability? Power spectra of the local film thickness $h(x_0,y_0,t)$ consist primarily of the fundamental frequency and *many* higher harmonics if f is not close to $f_c(R)$, so it may be difficult to explain this instability by using weakly nonlinear theory. For example, it is hard to understand why *only* troughs are strongly modulated, from the viewpoint of three or four wave interactions.

Floquet analysis has been applied to the secondary instability of film flows by Joo and Davis,[17] Trifonov,[26] and Chang *et al.*[23,28] Considering the 3-D disturbances as spatially growing, and letting $\xi = x - ct$, where c is the wave phase velocity, we can write the film thickness in the following form:

$$h(x,y,t) = h_2(\xi) + \epsilon H(\xi) \exp(\delta_r x + i\delta_i \xi + ik_y y), \tag{1}$$

with

$$H(\xi + \lambda_x) = H(\xi) = \sum_n c_n \exp(ik_x n\xi). \tag{2}$$

Here h_2 is the periodic 2-D wave, ϵ is the initial amplitude of spanwise modulations, and $k_x = 2\pi/\lambda_x$ and $k_y = 2\pi/\lambda_y$ are the streamwise and spanwise wave numbers, respectively. The real number δ_r is the spatial growth rate of a transverse normal mode with wave number k_y. For the synchronous 3-D instability $\delta_i = 0$; for a 3-D subharmonic instability $\delta_i = k_x/2$. By including *many* Fourier modes $\exp(ik_x n\xi)$, $H(\xi)$ can in principle account for the fact that only troughs are modulated.

Joo and Davis[17] studied the synchronous 3-D instability of nearly sinusoidal waves on vertically falling films by using a long wave evolution equation[20] that is valid for R close to R_c. Although the 2-D waves in our experiments are far from sinusoidal (Fig. 1), it is still worthwhile to compare our results with their predictions qualitatively. Joo and Davis found that 2-D waves are unstable to transverse modulations with sufficiently long spanwise wavelength (λ_y). Our observation of long wave ($\lambda_y \gg h_0$) spanwise modulations seems qualitatively similar. In the calculations, the most amplified spanwise wavelength decreases with increasing R for fixed f. This computational result also agrees with our measurements qualitatively [Fig. 10(a)].

However, the results of Joo and Davis also suggest that the most amplified spanwise wavelength should decrease with increasing streamwise wavelength (λ_x) for fixed R, contrary to our observations that λ_y does not seem to change with λ_x [Fig. 10(b)].[37] The contours of the 3-D structure they computed are also quite different from our observations. (Their modulation affects both peaks and troughs, for example.) This discrepancy may be due to the limited applicability of the long wave evolution equation in describing strongly nonlinear phenomena; some limitations of this equation have been noted elsewhere.[39–41]

C. Herringbone patterns—The three-dimensional subharmonic instability

1. Observations

The herringbone patterns result from a broad band of subharmonic resonances, as is implied by Fig. 5(b). To study these resonances in detail, we superposed small periodic disturbances at frequency $f/2 + \Delta f$ on the primary 2-D waves f at the entrance manifold, where f is in the subharmonic 3-D

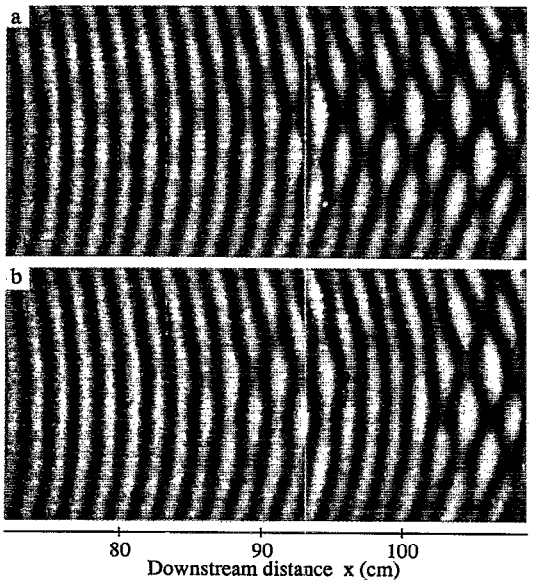

FIG. 12. Stabilized herringbone patterns generated by subharmonic and detuned disturbances. The experimental conditions are the same as those of Fig. 4, except for the weak secondary forcing; $\beta=4°$, $R=50.5$, and $f=14$ Hz. The secondary perturbation frequencies are (a) $f_1=f/2=7.0$ Hz; (b) $f_1=6.5$ Hz. The corresponding detuning parameters are (a) $\mu=0$ and (b) $\mu=0.0357$.

region of the phase diagram (Fig. 6). The initial power ratio is about 10^{-4}. We found that the herringbone patterns can be enhanced in all cases for which $|\Delta f|<f^*\approx f/6$. The patterns are the same for Δf and $-\Delta f$, so we define a "detuning parameter" $\mu=|\Delta f|/f$.

Three herringbone patterns resulting from this two-frequency forcing are shown in Fig. 12. These pictures were recorded under the same conditions as Fig. 4, except for the addition of a secondary forcing near the subharmonic frequency: $f_1=f/2=7.0$ Hz [Fig. 12(a)] or $f_1=6.5$ Hz [Fig. 12(b)]. When the perturbation frequency is exactly at the subharmonic frequency ($f/2$), the herringbone patterns grow steadily as the primary waves travel downstream; their amplitudes do not fluctuate in space and time. On the other hand, *when the perturbation is detuned from the subharmonic frequency, the herringbone patterns appear in patches and contain long wave modulations in the streamwise direction* [Fig. 12(b)]. The long wave modulation wavelength varies inversely with $|\Delta f|$, as one might expect. We also note a π transverse phase shift between neighboring patches in Fig. 12(b). Therefore, the detuned case cannot be viewed simply as a streamwise modulation of the perfectly resonant pattern in Fig. 12(a).

We measured power spectra of the local thickness at several positions along a centerline in Fig. 12. The dominant frequencies are found to be f and $f/2\pm\Delta f$. The peaks $f/2\pm\Delta f$ are sharp and of nearly equal strength. We determined the integrated area under each peak in the power spectrum and plot the areas as a function of x in Fig. 13 to illustrate the spatial evolution of the spectral power. The power at $f/2\pm\Delta f$ grows exponentially at first and then saturates. The power at f, on the other hand, decreases slightly with x. This

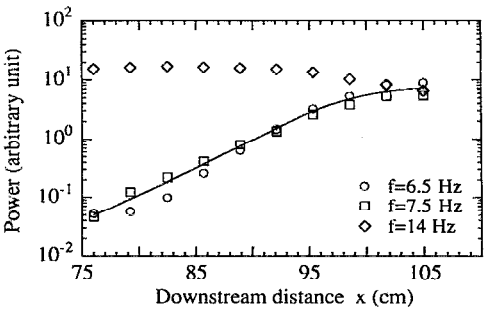

FIG. 13. Spatial evolution of the integrated spectral power along the centerline of Fig. 12(b), at the frequencies of certain spectral peaks. The peaks are located at $f=14$ Hz, $f_1=6.5$ Hz, and $f-f_1=7.5$ Hz, respectively. The solid line is a guide to the eye.

behavior is similar to that of the subharmonic instability in free shear layers.[7] The observations imply that the modulations extract *some* of their power from the primary waves. We determined the growth rate δ_i at $f/2\Delta f$ from the exponentially growing part of Fig. 13. The growth rate of the transverse modulations determined in this way does not vary significantly with Δf, for $|\Delta f|<f/6$.

For $|\Delta f|>f/6$, the 2-D sideband instability starts to appear instead.[22] The wave fronts are modulated transversely to some extent, but the well-developed herringbone patterns do not exist. When we superpose uniform white noise instead of periodic perturbations on the primary 2-D waves, the herringbone patterns can coexist with the 2-D sideband instability below a certain noise level. The power spectra of local thickness show both subharmonic and sideband peaks (not

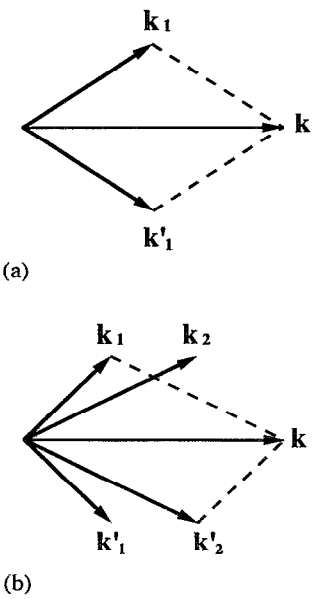

FIG. 14. (a) A subharmonic resonant triad that produces herringbone patterns: $\mathbf{k}_1+\mathbf{k}'_1=\mathbf{k}$, where $k_{1x}=k'_{1x}=k/2$. (b) The detuned case: two asymmetric resonant triads exist simultaneously. Here $\mathbf{k}_1+\mathbf{k}'_2=\mathbf{k}$ and $\mathbf{k}'_1+\mathbf{k}=\mathbf{k}$ (see the text for details).

shown). However, the herringbone patterns are often twisted in this case.

Measurements taken for various controlled and noncontrolled perturbations suggest that *the spectral width of the 3-D subharmonic resonances is approximately f/3, where f is the frequency of primary 2-D waves*. It is interesting to note that similar results were obtained by Kachanov and Levchenko[28] for the subharmonic transition in boundary layers. (For the Tollmien–Schlichting waves at $f=120$ Hz, Kachanov and Levchenko estimated the spectral width as 40 and 50 Hz for controlled and noncontrolled subharmonic perturbations, respectively.)

2. Theoretical description of the herringbone patterns

How do the patterns develop? Our experiments show that the primary 2-D waves can interact strongly with the fluctuations within a broad band of frequencies around the subharmonic. Chang *et al.*[23] proposed that for the nearly sinusoidal waves, a three-wave resonant interaction can give rise to a 3-D subharmonic instability and herringbone patterns. We use this model to explain qualitatively the development of these patterns under the influence of subharmonic and detuned perturbations. The phenomenon of subharmonic instability of boundary layers has been quantitatively explained in a similar way.[11,34]

The phase velocity depends on f,[21] so it seems difficult to satisfy the phase synchronism conditions (see Sec. II B) exactly for a broad band of frequency. However, as was pointed out by Zelman and Maslennikova,[34] exact phase synchronization is not a necessary requirement for the amplification of subharmonics; approximate synchronization may be sufficient. Second, we found that the herringbone patterns are stable over a long distance (20–$30\lambda_x$) before they turn into chaotic waves. This observation demonstrates that the phases of interacting waves may lock together.[32] Phase locking and synchronization depend on the fact that the dispersion relation is nearly linear.

The formation of the herringbone patterns is illustrated qualitatively in Figs. 14 and 15. We assume that the primary wave ($\mathbf{k}=k\hat{\mathbf{x}},f$) is sinusoidal, where $\hat{\mathbf{x}}$ is the streamwise unit vector, and that a small perturbation f_1 applied to the entrance manifold can generate both streamwise and oblique modes at f_1. Because of the inversion symmetry in the transverse direction, an oblique mode with a spanwise component $k_{1y}\hat{\mathbf{y}}$ should appear with another wave having the component $-k_{1y}\hat{\mathbf{y}}$ at the same time, where $\hat{\mathbf{y}}$ is the spanwise unit vector. Therefore, the small oblique modes are $(\mathbf{k}_1,f_1)=(k_{1x}\hat{\mathbf{x}}+k_{1y}\hat{\mathbf{y}},f_1)$ and $(\mathbf{k}_1',f_1)=(k_{1x}\hat{\mathbf{x}}-k_{1y}\hat{\mathbf{y}},f_1)$. If $f_1=f/2$ (and $k_{1x}=k/2$), the two oblique modes $(\mathbf{k}_1,f_1)$ and $(\mathbf{k}_1',f_1)$ form a resonant triad with the primary wave $(\mathbf{k},f)$, as shown in Fig. 14(a), and are strongly amplified downstream. *The 3-D waves are the superposition of the primary wave and resonant oblique waves that are growing spatially*:

$$h=A_0\exp[i(kx-2\pi ft)]+G(x)B_0\left\{\exp\left[i\left(\frac{k}{2}x+k_{1y}y-\pi ft\right)\right]+\exp\left[i\left(\frac{k}{2}x-k_{1y}y-\pi ft\right)\right]\right\}, \quad (3)$$

where A_0 is the amplitude of primary waves and B_0 is the initial amplitude of oblique modes. The factor $G(x)$ describes the spatial growth of the oblique waves. It has a similar shape to the solid curve in Fig. 13; the oblique waves first grow exponentially and then saturate. A snapshot of Eq. (3) is shown in Fig. 15(a), which closely resembles the experimental observation shown in Fig. 12(a). As we mentioned above, the perturbation f_1 also excites streamwise modes. However, our measurements show that *the oblique subharmonic modes grow much faster than the streamwise subharmonic modes.*

Detuning: If the secondary forcing frequency $f_1\neq f/2$, the initially generated oblique modes $(\mathbf{k}_1,f_1)$ and $(\mathbf{k}_1',f_1)$ cannot form a resonant triad with the fundamental 2-D wave $(\mathbf{k},f)$. However, the oblique mode $(\mathbf{k}_1,f_1)$ and the primary wave $(\mathbf{k},f)$ can form an asymmetric resonant triad with another oblique mode $(\mathbf{k}_2',f_2)=[(k-k_{1x})\hat{\mathbf{x}}-k_{1y}\hat{\mathbf{y}},f-f_1]$, as shown in Fig. 14(b). Therefore, the mode $(\mathbf{k}_2',f_2)$ emerges, and subsequently the two oblique modes, $(\mathbf{k}_1,f_1)$ and $(\mathbf{k}_2',f_2)$, are amplified downstream.[30,32] Similarly, $(\mathbf{k}_1',f_1)$ and $(\mathbf{k},f)$ can form a second resonant triad with $(\mathbf{k}_2,f_2)=[(k-k_{1x})\hat{\mathbf{x}}+k_{1y}\hat{\mathbf{y}},f-f_1]$. For the same detuning parameter as in Fig. 12(b), the superposition of the primary wave and the *four* spatially growing oblique waves gives rise to the simulated herringone patterns in Fig. 15(b). The close resemblance between Fig. 12 (experiment) and Fig. 15 (model) supports our view that the three-wave resonant interaction can explain the 3-D subharmonic instability.

Alternatively, following Herbert's arguments in Ref. 10, we can also obtain this result qualitatively using the Floquet language. There have been spirited debates as to which approach is more appropriate in the study of subharmonic instabilities in boundary layers (see Refs. 10, 11, 32 and 34). Kachanov[11] recently summarized the literature: both methods demonstrate quantitative agreement with experiments on the 3-D subharmonic instability of boundary layers.

Further evidence for the resonant triad model can be obtained by considering special circumstances under which only one of the two asymmetric resonant triads in Fig. 14(b) is amplified. In this case, an *asymmetric* herringbone pattern can appear. This triad may be selected by biased initial conditions when the symmetry in the spanwise direction is broken. (This happens occasionally and is hard to control.) An example is shown in Fig. 16. If the perturbation frequency is the subharmonic, the herringbone patterns are qualitatively the same as that of Fig. 12(a). However, when we detune the perturbation frequency, the patterns are twisted [Fig. 16(a)], and the long wave modulations seen in Fig. 12(b) do not occur. The lattice formed by the maxima in the herringbone patterns changes from rectangles to parallelograms, as shown in Fig. 16(b). We measured the two angles θ_1 and θ_2 defined in Fig. 16, and plot them as function of the perturbations frequency in Fig. 17. The solid lines are the calculations of θ_1 and θ_2 based on the asymmetric resonant triad [Fig. 14(b)] and the measured streamwise and spanwise wave numbers, k, k_{1y}. They are in agreement with the measured angles.

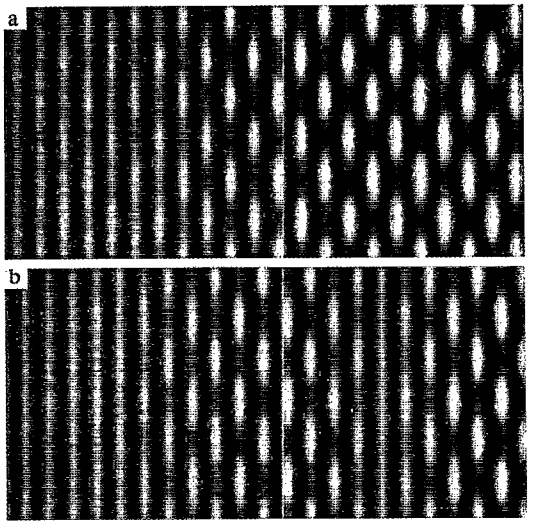

FIG. 15. Simulated herringbone patterns (see the text) for the detuning parameters in Fig. 12: (a) $\mu=0$ and (b) $\mu=0.0357$. These patterns resemble the experimental results shown in Fig. 12.

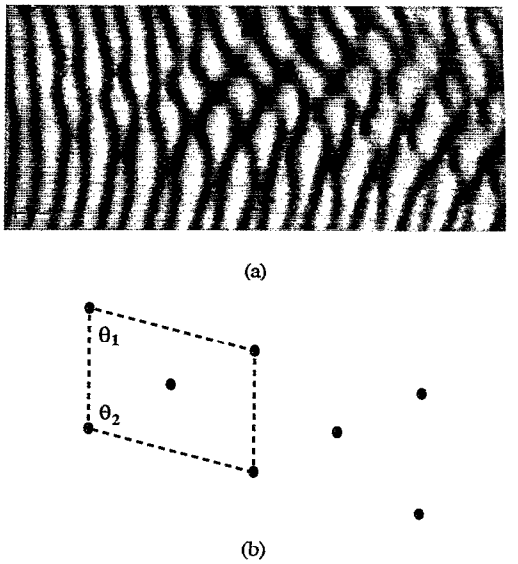

FIG. 16. (a) Experimental asymmetric herringbone patterns generated by one asymmetric resonant triad, where $\beta=4°$, $R=49.2$, $f=12$ Hz, and $f_1=5.1$ Hz. (b) Schematic lattice (a parallelogram) formed by the maxima of the herringbone patterns in (a).

The above arguments are qualitative and geometrical. Rigorous theoretical work is needed to fully understand the 3-D subharmonic instability mechanism. In the investigation of three-dimensional instabilities of vertically falling films, Chang *et al.*[23] found that the three-wave resonant interaction results in a 3-D subharmonic instability of nearly sinusoidal waves that is much like the one we observe for small inclination angles.

However, the instability occurs in a different region of parameter space than Chang *et al.*[23] apparently anticipated. [According to their calculations, the fundamental waves that are subject to the 3-D subharmonic instability are unstable to the 2-D subharmonic instability when the transverse noise level is low enough. *We found instead that the herringbone region (Fig. 6) is very close to $f_c(R)$, where the waves are subject to the 2-D sideband instability, rather than the 2-D subharmonic instability.*[22]] Chang *et al.* also predicted that the most amplified spanwise wave number decreases with increasing streamwise wave number of the fundamental waves, whereas we did not find a significant change of k_y with k_x in the experiments.[37] It is possible that these differences might be attributed to the fact that we use small inclination angles ($\beta=2.5°-7°$), while the computations assume $\beta=90°$ (vertical films). In another numerical study, Trifonov[26] predicted that the herringbone patterns can appear for the primary waves far below $f_c(R)$; this result is also contrary to our observations.

D. Further evolution of three-dimensional waves

The evolution of the 3-D waves after their inception involves the development and interaction of additional two- and three-dimensional modes. We present some qualitative observations in this section. *Far downstream, although the wave structure is essentially three dimensional, the solitary waves, which are largely two dimensional, become dominant eventually.* The spacings between the solitary waves and the shapes of the individual pulses are irregular.

We illustrate in Fig. 18 the downstream evolution of three-dimensional waves after the onset of the synchronous 3-D instability shown in Fig. 1. The experimental conditions are the same as those of Fig. 1. These snapshots were taken at successive donwnstream positions, but do not show literally the same waves. The film thickness *averaged over the spanwise direction*, $\langle h(x,y)\rangle_y/h_0$, is presented in Fig. 19 to show the development of streamwise structures.

As the waves travel downstream, the 2-D wave fronts break into nearly isolated depressions [Fig. 18(b)]. The waves become disorganized, and the two-dimensional structure, shown in the spanwise average of Fig. 19(b), is fairly weak. The flow becomes increasingly three dimensional [Fig. 18(c)]. However, the solitary wave structure soon be-

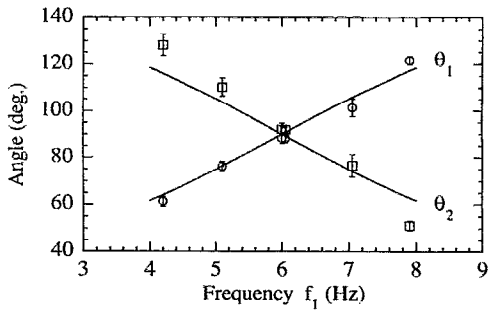

FIG. 17. Measurements of the angles θ_1 and θ_2 defined in Fig. 16(b) as functions of the secondary forcing frequency f_1. The solid curves are the calculations. The agreement supports our discussion of the herringbone patterns as resulting from nonlinear resonances.

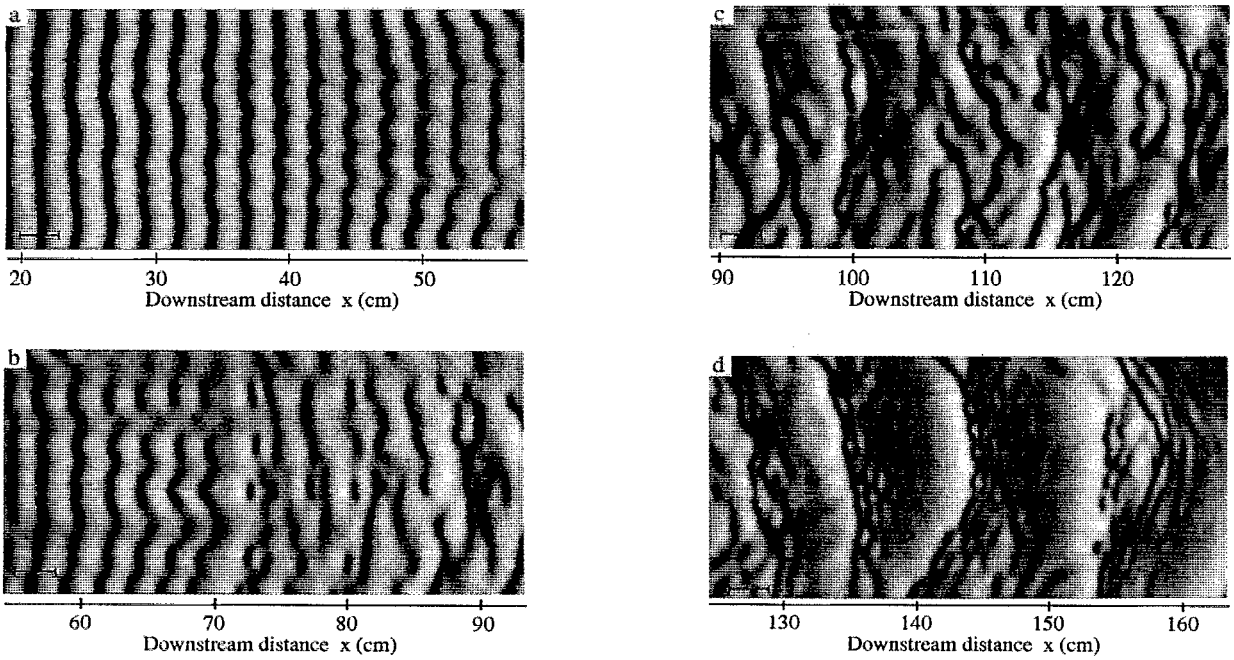

FIG. 18. Evolution of three-dimensional waves after the onset of the synchronous 3-D instability. Four snapshots are taken at successive downstream positions. The experimental conditions are the same as those of Fig. 1.

gins to grow out of the 3-D disordered motion [Fig. 19(c)]; the small waves preceding each solitary front are absorbed, in a process that is similar to what we previously noted for 2-D flows at higher viscosity.[21] The increasing dominance of the solitary waves with distance downstream is particularly obvious in the spanwise average [Fig. 19(d)].

The irregular spacing of these solitary pulses is on the average much larger than the initial primary wavelength. Though the solitary wave fronts are essentially three dimensional, they may be viewed perhaps as being locally two dimensional. *The solitary wave dynamics plays an important role in the further evolution of the turbulent film flows.* This observation is also applicable to the evolution after the onset of 3-D subharmonic instability.

V. CONCLUSION

A. Summary of the major results

The major results of this study of three-dimensional instabilities of film flows may be summarized as follows.

(1) Two distinct three-dimensional instabilities have been identified in different regions of the parameter space defined by the Reynolds number R and the frequency f of the fundamental 2-D waves (Fig. 6). The synchronous instability appears over a wide range of frequency, while the 3-D subharmonic instability (leading to herringbone patterns) occurs for frequencies close to the neutral curve $f_c(R)$. The synchronous transverse modulations maintain the streamwise periodicity of 2-D waves (Fig. 1). The herringbone patterns, on the other hand, double the period of 2-D waves, and the phase of the spanwise modulations differs by π for adjacent wave fronts (Fig. 4). The results for pure water and several glycerin solutions used in this experiment are qualitatively the same.

(2) The synchronous transverse modulations occur mainly along the trough regions of the primary 2-D waves (Fig. 7). The spanwise wavelength is much longer than the film thickness and comparable to the streamwise wavelength for moderate R. It turns out that this instability involves many higher harmonics of the fundamental waves, so Floquet analysis may be an appropriate theoretical method.

(3) The herringbone patterns result from a broad band of subharmonic resonances (Figs. 5 and 12). (These patterns may be viewed as two oblique waves resonating with the fundamental 2-D wave.) A similar process also occurs in boundary layers.[11] When the perturbation is detuned from the exact subharmonic frequency, the herringbone patterns appear in patches and are modulated in the streamwise direction. Herringbone patterns can be stabilized by perturbing the primary waves at the subharmonic frequency.

(4) The 3-D synchronous instability causes the wave fronts eventually to break up into (nearly) isolated depressions (Fig. 11). The subsequent evolution is complex [Figs. 18(b) and 18(c)].

(5) Far downstream, disordered solitary waves become dominant [Fig. 18(d)]. This happens for a wide range of parameters, no matter which 3-D instability initiates the growing complexity.

B. Concluding remarks

We have compared our observations with theoretical work on the three-dimensional instabilities in models of film flows.[17,23,26,38] While some predictions agree qualitatively with the present measurements, many of our observations

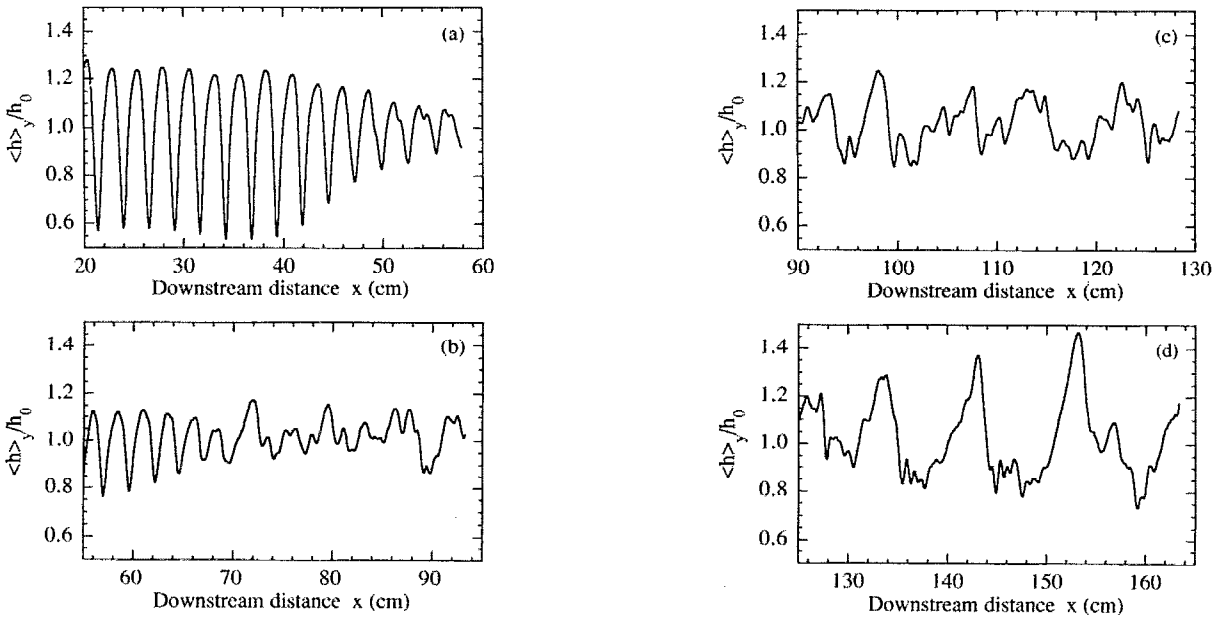

FIG. 19. Film thickness averaged in the spanwise direction, $\langle h(x,y)\rangle_y/h_0$, for the snapshots of Fig. 18. Strong 2-D structure largely disappears in (b) and (c), but returns as the solitary waves begin to dominate in (d).

remain to be explained. The synchronous 3-D instability merits special attention, since the most amplified waves resulting from the primary instability fall into this region of the 3-D instability phase diagram, so this process is especially important for natural (unforced) flows.

The three-dimensional instability mechanism depends on the nonlinear structure of the primary 2-D waves. When the fundamental waves are nearly sinusoidal, the process leading to three-dimensionality is weakly nonlinear, as in the case of the herringbone pattern of Fig. 4. On the other hand, when the primary wave profiles are far from sinusoidal, as in many of the other situations discussed in this paper (e.g., Figs. 1, 2, and 3), weakly nonlinear theory cannot be used. Similar observations have been made for boundary layers,[9] where the subharmonic instability usually dominates at small wave amplitudes and the synchronous K-type transition appears at large wave amplitudes.

A striking property of turbulent film flows is the eventual dominance of solitary pulses. The statistical properties of these disordered strongly nonlinear flows will be the subject of a subsequent paper in this series.

ACKNOWLEDGMENTS

We appreciate helpful discussions with H.-C. Chang. We also thank B. J. Gluckman for assistance, and W. S. Edwards and D. P. Vallette for suggestions on the manuscript. This work was supported by the National Science Foundation under Grant No. CTS-9115005.

[1]A. E. Dukler, "Characterization, effects and modeling of the wavy gas–liquid interface," in *Progress in Heat and Mass Transfer*, edited by G. Hetsroni, S. Sideman, and J. P. Hartnet (Pergamon, New York, 1972), Vol. 6, pp. 207–234.

[2]S. P. Lin and C. Y. Wang, "Modeling wavy film flows," in *Encyclopedia of Fluid Mechanics*, edited by N. P. Cheremisinoff (Gulf, Houston, 1985), Vol. 1, pp. 931–951.

[3]H.-C. Chang, "Wave evolution on a falling film," Annu. Rev. Fluid Mech. **26**, 103 (1994).

[4]P. L. Kapitza and S. P. Kapitza, "Wave flow of thin layers of a viscous fluid: III. Experimental study of undulatory flow conditions," Zh. Exp. Teor. Fiz. **19**, 105 (1949). Also in *Collected Papers of P. L. Kapitza*, edited by D. Ter Haar (Pergamon, London, 1965), Vol. 2, pp. 690–709.

[5]S. R. Tailby and S. Portalski, "The determination of the wavelength on a vertical film of liquid flowing down a hyrodynamically smooth plate," Trans. Inst. Chem. Eng. **40**, 114 (1962).

[6]S. V. Alekseenko, V. Y. Nakoryakov, and B. G. Polusaev, "Wave formation on a vertical falling liquid film," AIChE J. **31**, 1446 (1985).

[7]C.-M. Ho and P. Huerre, "Perturbed free shear layers," Annu. Rev. Fluid Mech. **16**, 365 (1984).

[8]J. C. Lasheras and H. Choi, "Three-dimensional instability of a plane free shear layer: An experimental study of the formation and evolution of streamwise vortices," J. Fluid Mech. **189**, 53 (1988).

[9]B. J. Bayly, S. A. Orszag, and T. Herbert,"Instability mechanisms in shear-flow transition," Annu. Rev. Fluid Mech. **20**, 359 (1988).

[10]T. Herbert, "Secondary instability of boundary layers," Annu. Rev. Fluid Mech. **20**, 487 (1988).

[11]Y. S. Kachanov,"Physical mechanisms of laminar-boundary-layer transition," Annu. Rev. Fluid Mech. **26**, 411 (1994).

[12]J. Liu, J. D. Paul, E. Banilower, and J. P. Gollub, "Film flow instabilities and spatiotemporal dynamics," in *Proceedings of the First Experimental Chaos Conference*, edited by S. Vohra, M. Spano, M. Shlesinger, L. M. Pecora, and W. Ditto (World Scientific, Singapore, 1992), pp. 225–239.

[13]C. S. Yih, "Stability of liquid flow down an inclined plane," Phys. Fluids **6**, 321 (1963).

[14]T. B. Benjamin, "Wave formation in laminar flow down an inclined plane," J. Fluid Mech. **2**, 554 (1957).

[15]P. Huerre and P. A. Monkewitz,"Local and global instabilities in spatially developing flows," Annu. Rev. Fluid Mech. **22**, 473 (1990).

[16]J. Liu, J. D. Paul, and J. P. Gollub,"Measurements of the primary instabilities of film flows," J. Fluid Mech. **250**, 69 (1993).

[17]S. W. Joo and S. H. Davis, "Instabilities of three-dimensional viscous falling films," J. Fluid Mech. **242**, 529 (1992).

[18]H. B. Squire, "On the stability for three-dimensional disturbances of viscous fluid flow between parallel walls," Proc. R. Soc. London Ser. A **142**, 621 (1993).

[19]T. B. Benjamin, "The development of three-dimensional disturbances in

an unstable film of liquid flowing down an inclined plane," J. Fluid Mech. **10**, 401 (1961).
[20]M. V. G. Krishna and S. P. Lin, "Nonlinear stability of a viscous film with respect to three-dimensional side-band disturbances," Phys. Fluids **20**, 1039 (1977).
[21]J. Liu and J. P. Gollub, "Solitary wave dynamics of film flows," Phys. Fluids **6**, 1702 (1994).
[22]J. Liu and J. P. Gollub, "Onset of spatially chaotic waves on flowing films," Phys. Rev. Lett. **70**, 2289 (1993).
[23]H.-C. Chang, M. Cheng, E. A. Demekhin, and D. I. Kopelevich, "Secondary and tertiary excitation of three-dimensional patterns on a falling film," J. Fluid Mech. **270**, 251 (1994).
[24]M. Cheng and H.-C. Chang,"Competition between subharmonic and sideband secondary instabilities on a falling film," preprint, 1994.
[25]M. Cheng and H.-C. Chang, "Stability of axisymmetric waves on liquid films flowing down a vertical column to azimuthal and streamwise disturbances," Chem. Eng. Commun. **118**, 327 (1992).
[26]Y. Y. Trifonov, "Bifurcations of two-dimensional into three-dimensional wave regimes for a vertically flowing liquid film," Izv. Akad. Nauk. SSSR. Mekh. Zhid. Gaza **5**, 109 (1990) [English translation, Fluid Dyn. **25**, 741 (1990)].
[27]R. E. Kelly, D. A. Goussis, S. P. Lin, and F. K. Hsu, "The mechanism for surface wave instability in film flow down an inclined plane," Phys. Fluids A **1**, 819 (1989).
[28]M. K. Smith, "The mechanism for the long-wave instability in thin liquid films," J. Fluid Mech. **217**, 469 (1990).
[29]P. S. Klebanoff, K. D. Tidstrom, and L. M. Sargent, "The three-dimensional nature of boundary-layer instability," J. Fluid Mech. **12**, 1 (1962).
[30]Y. S. Kachanov and V. Y. Levchenko,"The resonant interaction of disturbances at laminar-turbulent transition in a boundary layer," J. Fluid Mech. **138**, 209 (1984).
[31]R. E. Kelly, "On the stability of an inviscid shear layer which is periodic in space and time," J. Fluid Mech. **27**, 657 (1967).
[32]A. D. D. Craik, *Wave Interactions and Fluid Flows* (Cambridge University Press, London, 1985).
[33]J. L. Hammack and D. M. Henderson, "Resonant interactions among surface water waves," Annu. Rev. Fluid Mech. **25**, 55 (1993).
[34]M. B. Zelman and I. I. Maslennikova, "Tollmien–Schlichting-wave resonant mechanism for subharmonic-type transition," J. Fluid Mech. **252**, 449 (1993).
[35]Y. S. Kachanov, "On the resonant nature of the breakdown of a laminar boundary layer," J. Fluid Mech. **184**, 43 (1987).
[36]W. B. Krantz and S. L. Goren,"Stability of thin liquid films flowing down a plane," Ind. Eng. Chem. Fundam. **10**, 91 (1971).
[37]Possible reasons for the lack of frequency dependence of λ_y are: (a) the most amplified spanwise wavelength changes little with frequency for a fixed R; (b) an initial transverse modulation is relatively strong, and its growth rate is close to that of the most amplified perturbation, so it dominates the growth process.
[38]H.-C. Chang, E. A. Demekhin, and D. I. Kopelevich,"Nonlinear evolution of waves on a vertically falling film," J. Fluid Mech. **250**, 433 (1993).
[39]A. Pumir, P. Manneville, and Y. Pomeau, "On solitary waves running down an inclined plane," J. Fluid Mech. **135**, 27 (1983).
[40]S. W. Joo, S. H. Davis, and S. G. Bankoff, "Long-wave instabilities of heated falling films: Two-dimensional theory of uniform layers," J. Fluid Mech. **230**, 117 (1991).
[41]P. Rosenau and A. Oron,"Bounded and unbounded patterns of the Benney equation," Phys. Fluids A **4**, 1102 (1992).